Electronic Supplementary information: Quantitative, precise and multi-wavelength evaluation of the light-to-heat conversion efficiency for nanoparticular photothermal agents with calibrated photoacoustic spectroscopy

Théotim Lucas,[a,b,†] Clément Linger,[a,c,†] Thomas Naillon,[d,f] Mahshid Hashemkhani,[b] Lise Abiven,[b] Bruno Viana,[f] Corinne Chaneac,[d] Gautier Laurent,[e] Rana Bazzi,[e] Stéphane Roux,[e] Sonia Becharef,[b] Guilio Avveduto,[b] Florence Gazeau,[b] and Jérôme Gateau [a]*

[a.] *Sorbonne Université, CNRS, INSERM, Laboratoire d'Imagerie Biomédicale, LIB, F-75006, Paris, France. E-mail : jerome.gateau@sorbonne-universite.fr*
[b.] *Université Paris Cité, CNRS UMR 7057, Matière et Systèmes Complexes, MSC, F-75006 Paris, France.*
[c.] *Université Paris-Saclay, CNRS, Institut Galien Paris-Saclay, IGPS, F-91400 Orsay, France.*
[d.] *Sorbonne Université, CNRS UMR 7574, Laboratoire Chimie de la Matière Condensée de Paris, F-75005 Paris, France*
[e.] *Université de Franche-Comté, CNRS, Institut UTINAM, F-25000 Besançon, France*
[f.] *Chimie ParisTech, CNRS, PSLResearch University, Institut de Recherche de Chimie Paris, F-75231 Paris, France*
† *Théotim Lucas and Clément Linger contributed equally.*

Table of content

Photothermal model: link between the LHCE and the optical properties

To fully understand equation (1) and the link between the photothermal and photoacoustic equations, we need to derive again equation (1) from the energy balance at mesoscopic scale. For the sake of simplicity, we consider an illumination at the optical wavelength λ and a single kind of molecular or nanoparticular absorber. Generalization to multiple kinds of absorbers can be performed by applying the Beer–Lambert–Bouguer law. The absorber has an absorption cross section $\sigma_a(\lambda)$ (in m^2) and a density number $n(\boldsymbol{r},t)$ (in m^{-3}) at the position $\boldsymbol{r}$ and time t. The rate of optical energy absorbed and converted into heat for a single absorber can be written:

$$\delta\dot{Q}_{\,single\,absorber}(\boldsymbol{r},t) \;=\; \sigma_a(\lambda)\cdot\phi(\boldsymbol{r},t)\;\cdot \mathrm{E_{pt}}(\lambda) \qquad \text{(S 1)}$$

where $\phi(\boldsymbol{r},t)$ is the optical flux density or optical intensity (in $W.m^{-2}$) and $E_{pt}(\lambda)$ is the photothermal conversion efficiency (unit less). The photothermal conversion efficiency is the ratio of the energy effectively converted into a thermal increase of the solution to the total absorbed optical energy. E_{pt} may be inferior to 1, due to various competitive pathways such as fluorescence or photochemical reactions, for instance. The heat function $H(\boldsymbol{r},t)$ is the optical energy deposited as heat per unit volume and unit time at the position $\boldsymbol{r}$ and time t. For a colloidal suspension, $H(\boldsymbol{r},t)$ can be decomposed as the sum of the contributions of the continuous phase and dispersed phase:

$$H(\boldsymbol{r},t) \;=\; H_{continuous}(\boldsymbol{r},t) \;+ H_{dispersed}(\boldsymbol{r},t) \qquad \text{(S 2)}$$

$$H_{continuous}(\boldsymbol{r},t) = \;\mu_{continuous}(\lambda)\cdot\;\phi(\boldsymbol{r},t) \qquad \text{(S 3)}$$

$$H_{dispersed}(\boldsymbol{r},t) = n(\boldsymbol{r},t)\cdot\delta\dot{Q}_{single\,absorber}(\boldsymbol{r},t) = \mathrm{E_{pt}}(\lambda)\cdot\mu_a(\lambda,\boldsymbol{r},t)\cdot\;\phi(\boldsymbol{r},t) \qquad \text{(S 4)}$$

where $\mu_a = n\cdot\sigma_a$ is the absorption coefficient (in m^{-1}) of the dispersed phase and $\mu_{continuous}$ is the absorption coefficient of the continuous phase (in m^{-1}) for which we assume a photothermal conversion efficiency equal to 1. For samples considered for biomedical photothermal agents, the continuous phase is usually water.

The laser-induced rate of heat flow $\dot{Q}_I$ can be written as the integral over the illuminated volume of $H_{dispersed}(\boldsymbol{r},t)$. In the typical configuration modeled in PTT, a collimated laser beam is assumed to experience a unidirectional propagation (along an axis z) over a slab of thickness L (in m) (between z=0 and z=L) and with an incident surface S (in m^2) for a top-hat beam. For other types of

beam profiles, S is the integral of the normalized intensity distribution in the transverse plan. The illumination is also expected to be time-invariant. For a homogeneous solution, μ_a does not depend on the position and time and $\dot{Q}_I$ can be written:

$$\dot{Q}_I = S \cdot \int_0^L H_{dispersed}(z,t)\, dz = E_{pt}(\lambda) \cdot \mu_a(\lambda) \cdot S \cdot \int_0^L \phi(z)\, dz \quad \text{(S 5)}$$

The variation of the optical intensity with the coordinate z can be expressed with the attenuation coefficient $\mu_{att,\,solution}(\lambda)$ (in m^{-1}) which corresponds to the loss of intensity due to the absorption and the scattering of the solution:

$$\phi(z) = \frac{I_0}{S} \cdot e^{-\mu_{att,\,solution}(\lambda)\cdot z} \quad \text{(S 6)}$$

Therefore,

$$\dot{Q}_I = E_{pt}(\lambda) \cdot \frac{\mu_a(\lambda)}{\mu_{att,solution}(\lambda)} \cdot I_0 \cdot (1 - e^{-\mu_{att,solution}(\lambda)\cdot L}) \quad \text{(S 7)}$$

When the contribution of the continuous phase to the attenuation is considered negligible, the attenuation A_λ from the dispersed phase can be used:

$$\dot{Q}_I \approx E_{pt}(\lambda) \cdot \frac{\mu_a(\lambda)}{\mu_{att,\,solution}(\lambda)} \cdot I_0 \cdot (1 - 10^{-A_\lambda}) \quad \text{(S 8)}$$

From equation (1) and equation (S 8), the light-to-heat conversion efficiency can also be written:

$$\eta_T(\lambda) = E_{pt}(\lambda) \cdot \frac{\mu_a(\lambda)}{\mu_{att,\,solution}(\lambda)} \quad \text{(S 9)}$$

Equation (S 9) demonstrates that the light-to-heat conversion efficiency defined by the community of the photothermal therapy (PTT) is actually the product of the photothermal conversion efficiency E_{pt} of the solute and the ratio between the absorption coefficient of the solute and the attenuation coefficient of the solution.

A common practice in the PTT community is to determine the contribution of the continuous phase to the laser-induced rate of heat flow by performing a measurement of the heat flow with the continuous phase alone. However, with such an experiment for a non-scattering solvent like water, the heat flow is:

$$\dot{Q}_{continuous\ only} = I_0 \cdot (1 - e^{-\mu_{a,continous}(\lambda)\cdot L}) \quad \text{(S 10)}$$

$\dot{Q}_{continuous\ only}$ is larger than the integral of $H_{continuous}$ ($\boldsymbol{r}$,t), which is the actual contribution of the continuous phase and is equal to:

$$\dot{Q}_{continuous} = \frac{\mu_{a,continous}(\lambda)}{\mu_{att,solution}(\lambda)} \cdot I_0 \cdot (1 - e^{-\mu_{att,solution}(\lambda)\cdot L}) \quad \text{(S 11)}$$

Photoacoustic signal from the dispersed phase

For the nanosecond pulsed illumination, the optical intensity and the heat function (equation (S 2)) can be separated as $\phi(\boldsymbol{r},t) = \Phi(\boldsymbol{r}) \cdot f(t)$ and as $H(\boldsymbol{r},t) = \mathcal{H}(\boldsymbol{r}) \cdot f(t)$, respectively, where $f(t)$ is the temporal shape function with unit integral of the optical pulse, $\Phi(\boldsymbol{r})$ is the local fluence and $\mathcal{H}(\boldsymbol{r})$ is the local optical energy deposited as heat per unit volume. The generated acoustic pressure p (in Pa) measured at the detector position is considered to obey the wave equation[1]:

$$\left(\frac{\partial^2}{\partial t^2} - {c_w}^2 \cdot \nabla^2\right) p = p_0(\boldsymbol{r}) \cdot \frac{df(t)}{dt} \quad \text{(S 12)}$$

$$p_0(\boldsymbol{r}) = \frac{\beta}{C_p} \cdot c^2(\boldsymbol{r}) \cdot \mathcal{H}(\boldsymbol{r}) \quad \text{(S 13)}$$

where c_w is the sound speed (in $m.s^{-1}$) of the medium in which the acoustic wave propagates between the source and the detector. $p_0(\boldsymbol{r})$ is the initial acoustic pressure distribution induced by the optical energy deposition. β is the thermal expansion coefficient (in K^{-1}), C_p is the specific heat capacity (in $J.\ K^{-1}kg^{-1}$) and $c(\boldsymbol{r})$ is the local speed of sound (in $m.s^{-1}$) at the location of the optical energy

deposition. Equation (S 12) assumes a spatially uniform density of the propagation medium, and any effect of the viscosity is neglected. Moreover, the formula is valid under the condition of thermal confinement, which corresponds to a thermal conductivity taken to be zero during the acoustic emission (acoustic emission rapid compared with thermal diffusion)[1]. Equation (S 13) considers a condition of stress confinement[2] (acoustic emission is rapid compared to density change). All these conditions can be considered satisfied at the scale of the solution compartment in our experimental configuration.
The forward solution of equation (S 12) is[3] at the position $\boldsymbol{r}'$ and at the time t ($t > 0$, where t = 0 is the time of light pulse emission):

$$p(\boldsymbol{r}', t) = \iiint_{\substack{Illuminated \\ volume}} d^3\boldsymbol{r} \cdot \frac{1}{4 \cdot \pi \cdot {c_w}^2 \cdot |\boldsymbol{r}' - \boldsymbol{r}|} \cdot p_0(\boldsymbol{r}) \cdot \frac{d}{dt} f\left(t - \frac{|\boldsymbol{r}' - \boldsymbol{r}|}{c_w}\right) \quad \text{(S 14)}$$

We apply equation (S 14) to our spectroscopic system comprised of four tubes filled with the sample of interest, immersed in water and illuminated broadly. The volumetric integral of equation (S 14) corresponds to all the illuminated volume that comprises the solution within the tube, the tube itself and the illuminated volume of water around the tube. We can separate $p(\boldsymbol{r}', t)$ as the sum of the three contributions of the separated illuminated volumes.

$$p(\boldsymbol{r}', t) = p^{inside\ tube}(\boldsymbol{r}', t) + p^{tube}(\boldsymbol{r}', t) + p^{outside\ the\ tube}(\boldsymbol{r}', t) \quad \text{(S 15)}$$

The contribution inside the tube can even be separated between the contribution from the optically absorbing dispersed phase and the continuous phase:

$$p^{inside\ tube}(\boldsymbol{r}', t) = p^{dispersed}(\boldsymbol{r}', t) + p^{continuous}(\boldsymbol{r}', t) \quad \text{(S 16)}$$

Indeed, inside the tube, the initial pressure rises distribution for a uniform solution is obtained by combining the equations (S 2) and (S 13) :

$$p_0^{inside\ tube}(\boldsymbol{r}) = \left(\mathrm{E_{pt}}(\lambda) \cdot \mu_a(\lambda) + \mu_{continuous}(\lambda)\right) \cdot \Gamma_{solution} \cdot \Phi^{inside\ tube}(\boldsymbol{r}, \lambda) \quad \text{(S 17)}$$

$$\Gamma_{solution} = c_{solution}^2 \cdot \frac{\beta_{solution}}{C_{p,solution}} \quad \text{(S 18)}$$

where $\Gamma_{solution}$ is the dimensionless Grüneisen coefficient of the solution. Equation (S 17) assumes that the Grüneisen coefficient, and thereby the specific heat capacity and the thermal expansion generating the ultrasound signal, is the same for the continuous phase and for the optically absorbing dispersed phase.
The portion of the ultrasound waves that corresponds to the optically absorbing dispersed phase is:

$$p^{dispersed}(\boldsymbol{r}', t, \lambda) = \mathrm{E_{pt}}(\lambda) \cdot \mu_a(\lambda) \cdot \Gamma_{solution} \cdot \chi_0^{inside\ tube}(\boldsymbol{r}', t, \lambda) \quad \text{(S 19)}$$

$$\chi_0^{inside\ tube}(\boldsymbol{r}', t, \lambda) = \iiint_{\substack{Illuminated \\ tube}} d^3\boldsymbol{r} \cdot \frac{\Phi^{inside\ tube}(\boldsymbol{r}, \lambda)}{4 \cdot \pi \cdot {c_w}^2 \cdot |\boldsymbol{r}' - \boldsymbol{r}|} \cdot \frac{d}{dt} f\left(t - \frac{|\boldsymbol{r}' - \boldsymbol{r}|}{c_w}\right) \quad \text{(S 20)}$$

$\chi_0^{inside\ tube}(\boldsymbol{r}', t, \lambda)$ corresponds to the ultrasound waveform generated by the inside of the tube and measured at the position $\boldsymbol{r}'$.
To obtain the corresponding ultrasound signal, two linear operations have to be performed: a spatial integration on the detector to account for the spatial impulse response, and a temporal convolution to account for the electric impulse response of the detector. We note $\chi^{in\ tube}(\boldsymbol{r_i}, \mathrm{t}, \lambda)$ the waveform that incorporates the spatial and temporal response of the detector located at the position $\boldsymbol{r_i}$, the temporal profile of the optical excitation and its amplitude inside the tube.
The contribution of the optically absorbing dispersed phase to the ultrasound signal is then equal to:

$$s_i^{dispersed}(t, \lambda) = \mathrm{E_{pt}}(\lambda) \cdot \mu_a(\lambda) \cdot \Gamma_{solution} \cdot \chi^{in\ tube}(\boldsymbol{r_i}, \mathrm{t}, \lambda) \quad \text{(S 21)}$$

Similarly, the contribution of the continuous phase inside the tube to the ultrasound signal is then equal to:

$$s_i^{continuous}(t, \lambda) = \mu_{continuous}(\lambda) \cdot \Gamma_{solution} \cdot \chi^{in\ tube}(\boldsymbol{r_i}, \mathrm{t}, \lambda) \quad \text{(S 22)}$$

Uncertainty on the determination of the LHCE with photoacoustic spectrometry

First, we define how the values and the uncertainty are evaluated in our study from multiple measurements. To estimate a quantity from repeated experimental acquisitions, we use median because it is less sensitive to outliers than the mean. The median was notated:

$$\widetilde{\mathrm{X}} = \mathrm{median}(\mathrm{X}) \tag{S 23}$$

For the evaluation of the uncertainty, we used the median absolute deviation MAD, defined as:

$$MAD(X) = 1.4826 \times \mathrm{median}(|\mathrm{X} - \widetilde{\mathrm{X}}|) \tag{S 24}$$

The scale factor 1.4826 ensures that the value of MAD is comparable to the value of the standard deviation if the X values are normally distributed.
Then, the relative error was estimated using the following equation:

$$\frac{\Delta X}{X} \equiv \frac{MAD(X)}{\tilde{X}} \tag{S 25}$$

However, the median is also less efficient than the mean. To compute the relative error for the median value $\widetilde{X}$ evaluated with n measurements, we use the formula valid for a normal distribution of values:

$$\frac{\Delta \tilde{X}}{\tilde{X}} = \sqrt{\frac{\pi}{2 \cdot (\mathrm{n} - 1)}} \cdot \frac{\Delta X}{X} \tag{S 26}$$

Second, to evaluate the uncertainty on the determination of η_{PA}, the uncertainties have to be propagated over the different equations. From the theoretical equation (6), in practice, we compute η_{PA} by using $\tilde{\theta}^{PA}(\lambda)$.

$$\eta_{PA}(\lambda) = \frac{\tilde{\theta}^{PA}(\lambda)}{\mu_{att,\ dispersed}(\lambda)} \tag{S 27}$$

Since $\tilde{\theta}^{PA}(\lambda)$ and $\mu_{att,\ dispersed}(\lambda)$ are likely to be correlated the relative uncertainty can be estimated with the following equation:

$$\frac{\Delta \eta_{PA}}{\eta_{pA}} = \frac{\Delta \tilde{\theta}^{PA}(\lambda)}{\tilde{\theta}^{PA}(\lambda)} + \frac{\Delta \mu_{att,\ dispersed}(\lambda)}{\mu_{att,\ dispersed}(\lambda)} \tag{S 28}$$

We obtain $\theta^{PA}(\lambda)$ from the equations:

$$\theta^{PA}(\lambda) = \Psi^{PA}(\lambda) \cdot \mu_a^{calibration}(\lambda) \cdot {\eta_{PA}}^{calibration} \tag{S 29}$$

$$\Psi^{PA}(\lambda) = \frac{A^{PA}(\lambda)}{\tilde{A}^{PA}_{calibration}(\lambda)} \tag{S 30}$$

where $A^{PA}(\lambda)$ is the amplitude of the photoacoustic signal (after subtraction of the signal from the acquisition with the solvent only, and after projection in the image space for an improved signal-to-noise ratio) and $\tilde{A}^{PA}_{calibration}(\lambda)$ is the median value of the amplitude of the photoacoustic signal for the calibration solution of $CuSO_4$*$5H_2O$. For most experiments series of experiments performed here, n^{PA}_{calib} = 12 measurements for the calibration solution. ${\eta_{PA}}^{calibration}$ is the Light-to-Photoacoustic conversion efficiency of the calibration solution [4].

From equation (S 29), t

$$\frac{\Delta \theta^{PA}(\lambda)}{\theta^{PA}(\lambda)} = \frac{\Delta \Psi^{PA}(\lambda)}{\Psi^{PA}(\lambda)} + \frac{\Delta \mu_a^{calibration}(\lambda)}{\mu_a^{calibration}(\lambda)} + \frac{\Delta {\eta_{PA}}^{calibration}}{{\eta_{PA}}^{calibration}} \tag{S 31}$$

The measurements $A^{PA}(\lambda)$ and $\tilde{A}^{PA}_{calibration}(\lambda)$ can be considered as uncorrelated, therefore, from equation (S 30) we obtain:

$$\frac{\Delta\Psi^{PA}(\lambda)}{\Psi^{PA}(\lambda)} = \sqrt{\left(\frac{\Delta A^{PA}(\lambda)}{A^{PA}(\lambda)}\right)^2 + \left(\frac{\Delta\tilde{A}^{PA}_{calibration}(\lambda)}{\tilde{A}^{PA}_{calibration}(\lambda)}\right)^2} = \sqrt{\left(\frac{\Delta A^{PA}(\lambda)}{A^{PA}(\lambda)}\right)^2 + \frac{\pi}{2\cdot(n^{PA}_{calib}-1)}\cdot\left(\frac{\Delta A^{PA}_{calibration}(\lambda)}{A^{PA}_{calibration}(\lambda)}\right)^2} \quad \text{(S 32)}$$

${\eta_{PA}}^{calibration}$ is evaluated as the mean over the N = 25 wavelengths (680nm – 920 nm) of ${\eta_{0,PA}}^{calibration}(\lambda)$.

$${\eta_{0,PA}}^{calib} = \text{median}\left(\frac{\tilde{A}^{PA}_{calibration}(\lambda)}{A^{PA}_{ref\ nigrosin}(\lambda)}\right)\cdot\frac{\mu_a^{ref\ nigrosin}(\lambda)}{\mu_a^{calibration}(\lambda)} \quad \text{(S 33)}$$

Therefore, following equation (S 32)

$$\frac{\Delta{\eta_{0,PA}}^{calib}}{{\eta_{0,PA}}^{calib}} = \sqrt{\frac{\pi}{2\cdot(n^{PA}_{nigro}-1)}}\cdot\sqrt{\left(\frac{\Delta A^{PA}_{ref\ nigrosin}(\lambda)}{A^{PA}_{ref\ nigrosin}(\lambda)}\right)^2 + \frac{\pi}{2\cdot(n^{PA}_{calib}-1)}\cdot\left(\frac{\Delta A^{PA}_{calibration}(\lambda)}{A^{PA}_{calibration}(\lambda)}\right)^2} + \frac{\Delta\mu_a^{calibration}(\lambda)}{\mu_a^{calibration}(\lambda)} + \frac{\Delta\mu_a^{ref\ nigrosin}(\lambda)}{\mu_a^{ref\ nigrosin}(\lambda)} \quad \text{(S 34)}$$

and

$$\frac{\Delta{\eta_{PA}}^{calibration}}{{\eta_{PA}}^{calibration}} = \frac{1}{\sqrt{N}}\left(\frac{\Delta{\eta_{0,PA}}^{calib}}{{\eta_{0,PA}}^{calib}}\right) \quad \text{(S 35)}$$

The uncertainty of the spectrophotometer (VWR P4 Spectrophotometer, VWR, Leuven, Belgium) used to determine $\mu_a^{calibration}(\lambda)$ and $\mu_a^{ref\ nigrosin}(\lambda)$ is evaluated by the manufacturer to : $\frac{\Delta\mu_a(\lambda)}{\mu_a(\lambda)} \approx 0.4\ \%$ at absorbance 1. Since with the absorbance with the 2 mm-length cuvette is on the order of 0.2 and in agreement with the literature[5], we consider that a relative uncertainty of $\frac{\Delta\mu_a(\lambda)}{\mu_a(\lambda)} \approx 1\%$ reasonably correspond to our experiment.

Figure S1 (a) shows that the relative uncertainty $\frac{\Delta A^{PA}_{calibration}(\lambda)}{A^{PA}_{calibration}(\lambda)}$ can be taken equal to 3%. Figure S1 (b) shows that the relative uncertainty $\frac{\Delta A^{PA}_{ref\ nigrosin}(\lambda)}{A^{PA}_{ref\ nigrosin}(\lambda)}$ can be taken equal to 4%.Therefore, for n^{PA}_{nigro}= 20 and $n^{PA}_{calib} = 12$, equation (S 34) leads to $\frac{\Delta{\eta_{0,PA}}^{calib}}{{\eta_{0,PA}}^{calib}} = 3{,}2\%$ and equation (S 35) to $\frac{\Delta{\eta_{PA}}^{calibration}}{{\eta_{PA}}^{calibration}} = 0.64\%$. With the determined value of ${\eta_{PA}}^{calibration}$ (Figure S1(c)), we verified that the photoacoustic coefficient $\theta^{PA}(\lambda)$ obtained with equation (S 29) matches the absorption coefficient $\mu_a^{ref\ nigrosin}(\lambda)$.

Using the values above and for a total of n_{acq} measurements (including the 4 tubes), the relative error of η_{PA} for a compound other than the reference solution can be computed as:

$$\frac{\Delta\eta_{PA}}{\eta_{PA}}(\%) = \sqrt{\frac{\pi}{2\cdot(n_{acq}-1)}}\cdot\left(\sqrt{\left(\frac{\Delta A^{PA}(\lambda)}{A^{PA}(\lambda)}\right)^2 + \frac{\pi\cdot 9}{2\cdot 11}} + 1 + 0.64\right) + 1 \quad \text{(S 36)}$$

Typically, for $n_{acq} = 12$ measurements, and $\frac{\Delta A^{PA}(\lambda)}{A^{PA}(\lambda)}$ = 5% -10%, we obtain $\frac{\Delta\eta_{PA}}{\eta_{PA}} \approx 4\% - 6\%$

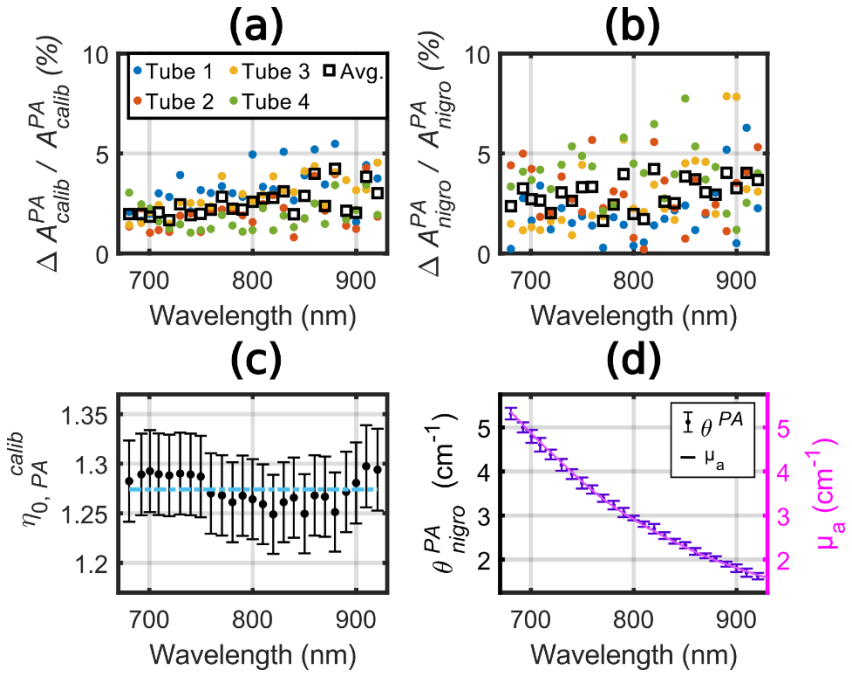

Figure S1: Variability for the two reference solutions and estimation of the LPCE of the calibration solution ($CuSO_4$). (a-b) Ratio of the MAD and the median value of (a) $A^{PA}_{calibration}(\lambda)$ over 12 acquisitions in 4 tubes and (b) $A^{PA}_{ref\ nigrosin}(\lambda)$ over 5 acquisitions in 4 tubes. The ratio was computed for each tube and each optical wavelength, and it is expressed in percentage. The average over the 4 tubes was computed (square markers). (c) ${\eta_{0,PA}}^{calib}$ computed with equation (S 33). The error bars were computed from equation (S 34) correspond to a relative error of ± 3.2 %. This value was obtained by considering n^{PA}_{nigro}= 20 , $\frac{\Delta A^{PA}_{ref\ nigrosin}(\lambda)}{A^{PA}_{ref\ nigrosin}(\lambda)} = 4\%$, $n^{PA}_{calib} = 12$ and $\frac{\Delta A^{PA}_{calibration}(\lambda)}{A^{PA}_{calibration}(\lambda)} = 3\%$. The mean over the 25 wavelength is plotted with the blue dashed line and corresponds to ${\eta_{PA}}^{calibration}$. (d) The photoacoustic coefficient (median ± MAD) obtained from equation (S 29) for the left axis and the absorption coefficient $\mu_a^{ref\ nigrosin}(\lambda)$ (right axis).

Characterization of the silver sulphide nanoparticles

Table S1. TEM and Hydrodynamic (Hy) mean diameters, quantum yield and suspension mass concentration of silver sulphide nanoparticles for both DTDTPA and MUA ligands.

Ag_2S Nanoparticles		TEM particle size (nm)	Dh-number (nm)	Dh-Intensity (nm)	Quantum yield (%)
Prepared with low $AgNO_3$ concentration	Ag_2S@MUA_{Low}	5.2 ± 1.7 nm	21.4	123	1.9 %
	Ag_2S@$DTDTPA_{Low}$	2.3 ± 0.6 nm	-	-	< 1 %
Prepared with high $AgNO_3$ concentration	Ag_2S@MUA_{High}	5.8 ± 1.3 nm	40.5	168	28 %
	Ag_2S@$DTDTPA_{High}$	4.3 ± 0.8 nm	41.5	421	1.6 %

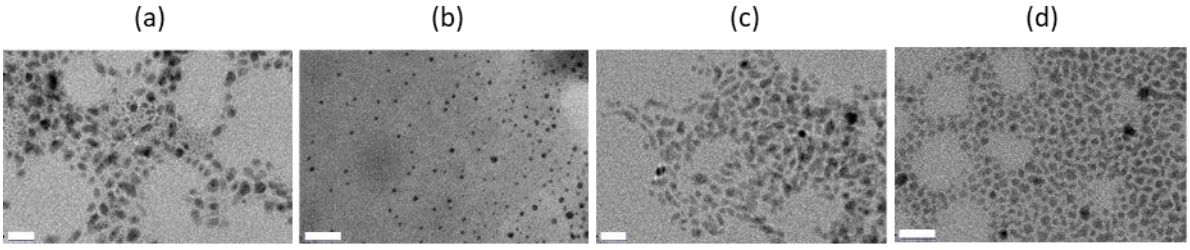

Figure S2. TEM images of Ag2S@MUALow (a), Ag2S@DTDTPALow (b), Ag2S@MUAHigh (c), Ag2S@DTDTPAHigh (d). Scale bare = 20 nm. Samples were prepared by dropping colloidal suspensions onto a copper grid coated with a carbon film and allowing the water to evaporate in air. The TEM images were obtained using a TecnaiSpiritG2 microscope operating at 120 kV. Size distribution histograms were obtained by measuring at least 150 particles per sample using the ImageJ software.

Characterization of the maghemite nanoflowers

Table S2. Core size (determined by TEM) and hydrodynamic diameter (Dh) of gold nanoparticles (Au@DTDTPA), of maghemite nanoflowers (γ-Fe_2O_3) and of maghemite nanoflowers decorated with Au@DTDTPA nanoparticles (γ-Fe_2O_3-Au).

Nanoparticles	Au@DTDTPA	γ-Fe_2O_3	γ-Fe_2O_3-Au
TEM particle size (nm)	2.3 ± 0.3	41.1 ± 4.0	42.9 ± 4.0
Dh (nm)	8.3 ± 2.1	45.0 ± 0.5	81.1 ± 0.8

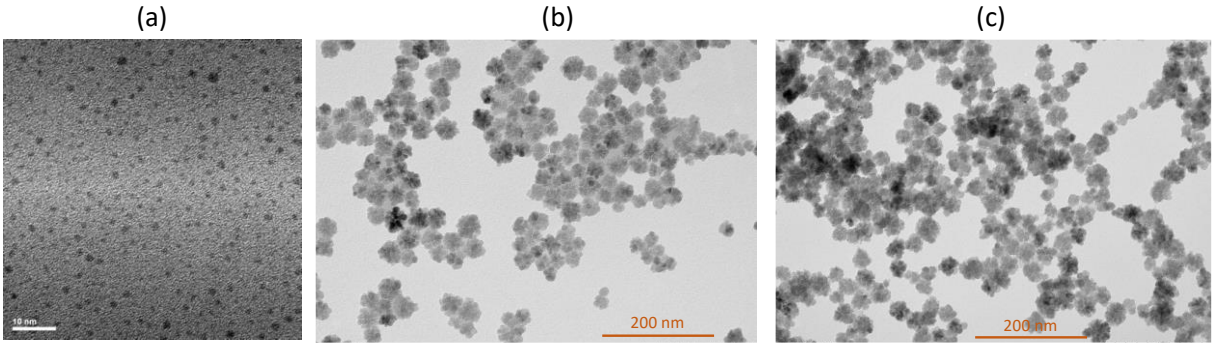

Figure S3. TEM micrographs of (a) gold nanoparticles (Au@DTDTPA, scale bar: 10 nm), (b) maghemite nanoflowers (γ-Fe_2O_3, scale bar: 200 nm) and (c) maghemite nanoflowers decorated with Au@DTDTPA nanoparticles (γ-Fe_2O_3-Au , scale bar: 200 nm). The size of the gold core, of γ-Fe_2O_3 and of γ-Fe_2O_3-Au was obtained from transmission electron microscopy (TEM) performed with a JEOL JEM 2100F microscope at 200 kV (ICB, Dijon, France). Drops of colloidal solutions were deposited on dedicated TEM carbon grids and observed after natural drying at room temperature. The size of the nanoparticles and nanoflowers were obtained by the average of the size of approximately 100 nanoparticles measured on different images.

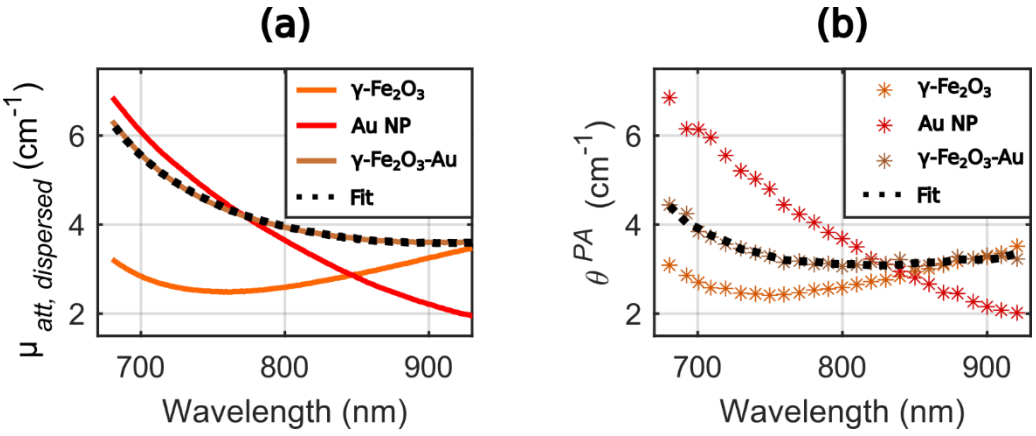

Figure S4: Spectral decomposition of the spectra of the γ-Fe_2O_3-Au sample as a linear sum of the spectra of the γ-Fe_2O_3 and Au NP samples. (a) The attenuation spectrum of the γ-Fe2O3-Au sample could be decomposed in a linear sum of the attenuation spectra of the γ-Fe_2O_3 and Au NP samples with weights 0.71 and 0.52, respectively. (b) The photoacoustic spectrum of the γ-Fe2O3-Au sample could be decomposed in a linear sum of the photoacoustic spectra of the γ-Fe_2O_3 and Au NP samples with weights 0.79 and 0.29, respectively. Here, the median of the photoacoustic coefficients was used. The decomposition was performed with a nonnegative linear least-squares solver.

References

1 B. Wu, C. Frez and G. J. Diebold, *Appl. Phys. Lett.*,2013 , DOI:10.1063/1.4821739.

2 B. Cox, J. G. Laufer, S. R. Arridge and P. C. Beard, *J. Biomed. Opt.*, 2012, **17**, 061202.

3 M. Xu and L. V. Wang, *Rev. Sci. Instrum.*, 2006, **77**, 1–22.

4 T. Lucas, M. Sarkar, Y. Atlas, C. Linger, G. Renault, F. Gazeau and J. Gateau, *Sensors*, 2022, **22**, 6543.

5 J. Galbán, S. De Marcos, I. Sanz, C. Ubide and J. Zuriarrain, *Anal. Chem.*, 2007, **79**, 4763–4767.